Effects of Different Quantum Coherence on the Pump–Probe Polarization Anisotropy of Photosynthetic Light-Harvesting Complexes: A Computational Study

ARTICLE *in* JOURNAL OF PHYSICAL CHEMISTRY LETTERS · MAY 2015

Impact Factor: 7.46 · DOI: 10.1021/acs.jpclett.5b00690

3 AUTHORS, INCLUDING:

Shuming Bai
Aix-Marseille Université
12 PUBLICATIONS **49** CITATIONS
SEE PROFILE

Qiang Shi
Chinese Academy of Sciences
101 PUBLICATIONS **2,419** CITATIONS
SEE PROFILE

THE JOURNAL OF PHYSICAL CHEMISTRY Letters

Letter

pubs.acs.org/JPCL

Effects of Different Quantum Coherence on the Pump–Probe Polarization Anisotropy of Photosynthetic Light-Harvesting Complexes: A Computational Study

Shuming Bai, Kai Song, and Qiang Shi*

Beijing National Laboratory for Molecular Sciences, State Key Laboratory for Structural Chemistry of Unstable and Stable Species, Institute of Chemistry, Chinese Academy of Sciences, No. 2 North 1st Street, Zhongguancun, Beijing 100190, China

ABSTRACT: Observations of oscillatory features in the 2D spectra of several photosynthetic complexes have led to diverged opinions on their origins, including electronic coherence, vibrational coherence, and vibronic coherence. In this work, effects of these different types of quantum coherence on ultrafast pump–probe polarization anisotropy are investigated and distinguished. We first simulate the isotropic pump–probe signal and anisotropy decay of the Fenna–Matthews–Olson (FMO) complex using a model with only electronic coherence at low temperature and obtain the same coherence time as in the previous experiment. Then, three model dimer systems with different prespecified quantum coherence are simulated, and the results show that their different spectral characteristics can be used to determine the type of coherence during the spectral process. Finally, we simulate model systems with different electronic-vibrational couplings and reveal the condition in which long time vibronic coherence can be observed in systems like the FMO complex.

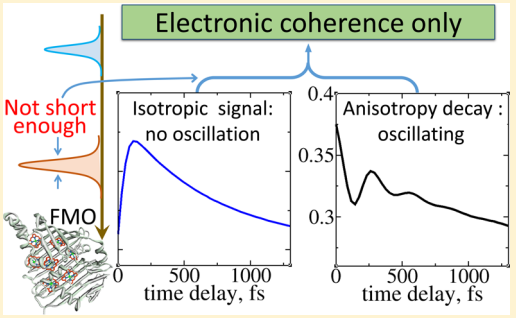

Highly efficient excitation energy transfer (EET) in photosynthetic complexes is crucial to generate the near-unity quantum efficiency of light harvesting and has attracted many research interests over the past decades.[1−3] The recently observed long-time quantum coherence features in the 2D spectra in photosynthetic complexes,[4−9] as well as in single light-harvesting complexes,[10] have initialized a wide discussion on their origins and the possible roles of quantum coherence in the highly efficient EET in biological photosynthesis. The initial explanation of the quantum beats in the 2D electronic spectra of the FMO complex is that they are due to the electronic coherence between different pigments,[4] which is further supported by simulations of the EET dynamics with the initial excitation localized on one of the pigments;[11] however, because the third-order optical response functions, rather than the population dynamics between different sites, are directly measured in the 2D spectra experiments, further studies are still needed to identify the links between the quantum beating signals in 2D spectra and the simulated coherent population dynamics.

The electronic coherence explanation has been questioned due to the reason that the strong coupling of electronic transitions to the condensed phase environment will result in decoherence within a few hundred femtoseconds. The mechanisms of vibrational or vibronic coherences are then proposed because the vibrational coherence can usually last much longer due to the weak coupling of the vibrational motion to the protein environment.[12−18] Vibronic coherence have been observed in recent 2D spectra studies of a cyanine dimer[19] and the photosystem II reaction center;[9] however, an important difference between the cyanine molecule and the bacteriochlorophyll *a* (Bchl*a*) molecule in photosynthetic light-harvesting complexes is that the Huang–Rhys factors of the latter are much smaller,[20,21] which is unlikely to produce significant quantum beats, as in ref 19. Indeed, a recent 2D spectra experiment by Fransted et al.[22] on isolated Bchl*a* molecules shows features very different from that of the FMO complex and thus excludes the possibility of intramolecular vibrational modes playing a major role.

Chen et al. have simulated the 2D spectra of the FMO complex at 77 K using a model with only electronic coherence,[23] and the calculated coherence time of ∼400 fs is significantly shorter than that obtained from the most recent experiment (longer than 1 ps).[6] It is interesting to note that the calculated coherence time is more similar to that observed in a previous pump–probe polarization anisotropy experiment.[24] Ultrafast pump–probe spectroscopy is another important method that has been used to study the quantum coherences by observing quantum beats originated from simultaneous excitation of multiple eigenstates. Characteristics of pump–probe signal have been used to determine which kind of the coherence exists. For example, Savikhin et al.[24] have used ultrafast polarization anisotropy experiments to demonstrate the existence of electronic coherence in the FMO complex of *C. Tepidum* at 19 K. Jonas and coworkers have studied vibrational and vibronic coherences in pump–probe polarization aniso-

Received: April 2, 2015
Accepted: May 8, 2015

DOI: 10.1021/acs.jpclett.5b00690
J. Phys. Chem. Lett. 2015, 6, 1954−1960

tropy signals of different systems, including dimer with Jahn–Teller coupling[25] and square symmetric molecule with conical intersections.[26] More recently, Yuen-Zhou et al. have suggested to use broadband pump/broadband probe spectra in distinguishing electronic coherence oscillation from vibronic-only oscillation in model dimers.[27] It is thus interesting to investigate theoretically the quantum coherences observed in the FMO complex by the ultrafast polarization anisotropy experiment and to further explore the experimental methods to distinguish different types of quantum coherence.

In this work, we study theoretically the effect of different types of quantum coherence on the pump–probe polarization anisotropy signals of photosynthetic complexes with a non-perturbative treatment of both the light–molecule interaction and the system–environment coupling, which has many advantages over the perturbative treatments in the so-called intermediate coupling regime.[2,28] We first simulate the signals of a FMO complex model with only electronic coherence and compare the results with the experiment by Savikhin et al.[24] Then, by simulating model dimer systems with different parameters, we show that quantum beats caused by different types of quantum coherence can be distinguished from their characteristic signals. Finally, by using a model dimer consisting of pigment 3 and 4 of the FMO complex, we show that whether the vibronic coherence can be observed depends on both the electron–phonon coupling strength and the laser pulse that needs to excite simultaneously more than one vibrational state.

We start from simulating the experimental pump–probe polarization anisotropy signals of the FMO complex of *C. Tepidum* at 19 K by Savikhin et al., where the electronic coherence was first observed.[24] In the experiment, the isotropic pump–probe signal $\Delta A_{iso}(t)$ ($\Delta A_{MA}(t)$ in ref 24) showed no obvious oscillations, while the anisotropy decay $r(t)$ showed quantum beats up to 0.5 ps depending on the pump and probe wavelength. The parallel and perpendicular pump–probe signals $\Delta A_{\parallel}(t)$ and $\Delta A_{\perp}(t)$ also showed oscillatory patterns that were similar to $r(t)$, but no longer time quantum beats that are usually associated with vibrational coherence were observed. Here the absorption spectra and pump–probe signals of the FMO complex are simulated by employing the parameters from previous works.[23,29,30] The Debye spectral density in eq 6 is used with η = 70 cm^{-1}, and ω_c^{-1} = 100 fs. Because the Debye spectral density describes an overdamped electronic-vibrational coupling, only electronic coherence can be observed in this model. The current model also assumes that fluctuations of the site energies on each pigments are uncorrelated. The possibility of correlated excitation energy fluctuations has been discussed in experimental[31] and theoretical[32−34] studies. Recently, Tiwari et al. have also proposed a model in which two chromophores in the photosynthetic complex may have anticorrelated coupling with a common underdamped vibrational mode;[12] however, recent molecular dynamics (MD) simulations combined with quantum-chemistry calculation have shown that no obvious correlations of excitation energy fluctuation can be observed during the time scale of the MD simulation.[21,35] This could be due to the weak interactions between the Bchla pigments, so correlated dynamical disorder is not considered in this work.

The absorption spectrum of the FMO complex at 19 K calculated with the model is shown in Figure 1, which agrees well with the experimental result.[24] The simulated parallel and perpendicular pump–probe signals as well as isotropic pump–probe signal $\Delta A_{iso}(t)$ and anisotropy decay $\Delta A_{\parallel}(t)$ and $\Delta A_{\perp}(t)$ of the FMO complex at 19 K are shown in Figure 2. The pump-and-probe wavelength is set to 820 nm, and the full width at half-maximum (fwhm) of the laser pulse is 87 fs. The results agree well with the experiment,[24] where the anisotropy decay signal shows quantum beats with a period of 240 fs corresponding to the energy difference between the lowest two exciton peaks. The absence of any obvious oscillations in the isotropic signal and the coherence time around 500 fs in the anisotropy decay also agree well with the experiment. We note that the simulation is performed at the low temperature of 19 K to compare with the experiment,[24] and it is expected that the amplitude of oscillations and the coherence time will be greatly reduced if the temperature is close to room temperature due to the much stronger decoherence caused by the dynamical disorder.

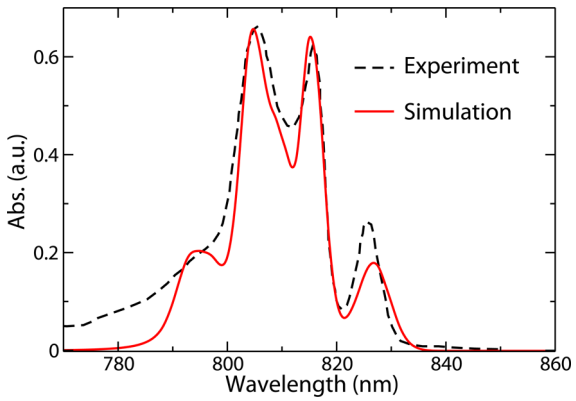

Figure 1. Simulated absorption spectra of the FMO complex at 19 K (solid line, red), compared with the experimental results from ref 24(dashed line, black).

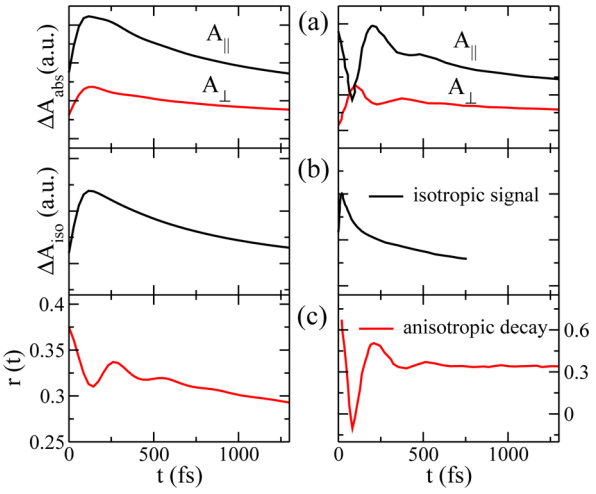

Figure 2. Comparison of simulated (left panel) and experimental (right panel) results for the FMO complex at 19 K: (a) polarized absorption difference $\Delta A_{\parallel}(t)$ and $\Delta A_{\perp}(t)$, (b) isotropic absorption difference, and (c) polarization anisotropy decay. The experimental results are taken from ref 24.

There are also some notable differences between results from the simulation and experiment: (1) The simulated oscillation amplitudes in $\Delta A_{\parallel}(t)$, $\Delta A_{\perp}(t)$, as well as $r(t)$ are smaller than the experiment. The most likely reason could be that there is too much decoherence for the first exciton peak as shown in Figure 1, which could be due to too large static or dynamic

DOI: 10.1021/acs.jpclett.5b00690
J. Phys. Chem. Lett. 2015, 6, 1954−1960

disorders used for pigment 3 (the major component of the first exciton state). Another possible reason could be due to the simplified Debye spectral density used in the simulation, which could be tested in future studies with more complex spectral densities calculated in realistic systems.[21,35,36] (2) The initial part of the anisotropy decay in the experiment (figure 1 of ref 24) shows some discontinuity and unusually large anisotropy values (much larger than 0.4 from the theoretical prediction in refs 25 and 37), which could be due to some coherent artifacts caused by the overlap and resonance of the pump and probe pulses.[38−40]

A main drawback of the above model is that no underdamped or undamped vibrational modes are included. Although the Huang−Rhys factors for the Q_y transition of the Bchla molecule are small (<0.05),[20,41] it is desirable to investigate their possible effects on the pump−probe polarization anisotropy. Simulation of the FMO complex at the low temperature of 19 K including additional underdamped or undamped vibrational modes is still very computationally demanding because of the large number of auxiliary reduced density operators (ADOs) needed to obtain converged results using the HEOM method. So simplified dimer models are employed to study their effects.

We use a model dimer configuration where the transition dipoles of the two monomers are perpendicular to each other. Such arrangement of the transition dipoles is close to the case of pigments 3 and 4 in the FMO complex, which has the lowest site energies (see below), and has nearly perpendicular transition dipole moments (107°). The difference between site energy of the two monomers is assumed to be ϵ = 200 cm^{-1}, and the simulation is performed at 77 K. Three different sets of parameters for the electronic coupling J and electronic−vibrational coupling are utilized to feature different types of quantum coherence: (1) The coupling between the two monomers is set to J = −200 cm^{-1}, and the vibrational motion is assumed to be overdamped, as described by the Debye spectral density in eq 6 with a characteristic decay time of ω_c^{-1} = 100 fs, so that only electronic coherence exists. (2) The vibrational mode is described by an underdamped harmonic oscillator with the Lorentzian spectral density in eq 7, the vibrational frequency ω_0 = 200 cm^{-1}, and the decaying constant γ = 20 cm^{-1}. The coupling J is set to zero so that only vibrational coherence exists. (3) The electronic coupling is set to J = −200 cm^{-1}, and the underdamped harmonic oscillator is taken with the same parameters as in case (2). Vibronic coherence arises because electronic coherence and the underdamped vibrational motions are coupled in this model. Parameters for the three models featuring different types of quantum coherence are summarized in Table 1. We note that the site energy difference and intermolecular coupling are similar to typical values found in some photosynthetic complexes, and a smaller vibrational frequency of 200 cm^{-1} is employed to help distinguish the vibrational and electronic quantum beats.

Table 1. Site Energy Difference ϵ (in cm^{-1}), Intermolecular Electronic Coupling J (in cm^{-1}), and Type of the Spectral Density Used in the Three Dimer Models Described in Cases (1)−(3)[a]

	ϵ	J	spectral density
Case (1)	200	−200	Debye (ω_c^{-1} = 100 fs)
Case (2)	200	0.0	Lorentzian (ω_0 = 200 cm^{-1}, γ = 20 cm^{-1})
Case (3)	200	−200	Lorentzian (ω_0 = 200 cm^{-1}, γ = 20 cm^{-1})

[a] η = 120 cm^{-1} for all three models.

In all three cases, reorganization energy of 60 cm^{-1} is used to describe the strength of the electronic-vibrational interaction in each monomer. In cases (2) and (3), this corresponds to a Huang−Rhys factor of 0.3. Gaussian distribution with an fwhm of 100 cm^{-1} on site energies is adopted to describe the static disorder. We set the frequency of both the pump and probe pulses to the average of the two site energies and the fwhm of the laser pulses to 50 fs.

The simulated polarized absorption differences $\Delta A_{\parallel}(t)$ and $\Delta A_{\perp}(t)$ of the above model dimers are shown in Figure 3, while

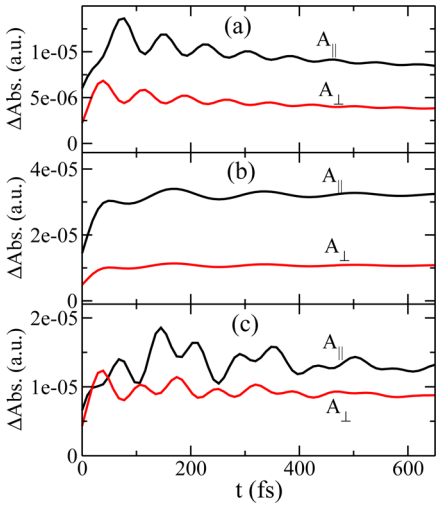

Figure 3. Polarized absorption differences $\Delta A_{\parallel}(t)$ and $\Delta A_{\perp}(t)$ of the model dimer at 77 K: (a) Case (1) with only electronic coherence, (b) Case (2) with only vibrational coherence, and (c) Case (3) with vibronic coherence.

the isotropic pump−probe signal $\Delta A_{iso}(t)$ and anisotropy decay $r(t)$ are shown in Figure 4. It can be seen that although all the time-dependent absorption differences oscillate in the three cases, the isotropic pump−probe signal and anisotropy decay signal show dramatic differences. In case (1), where only

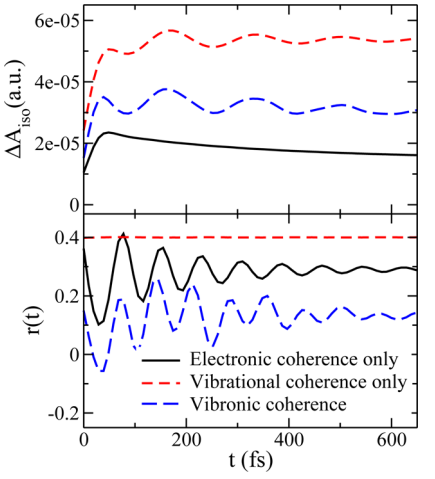

Figure 4. (a) Isotropic pump−probe signal $\Delta A_{iso}(t)$ and (b) the anisotropy decay signal $r(t)$ for the three-model dimer systems featuring different types of quantum coherence.

DOI: 10.1021/acs.jpclett.5b00690
J. Phys. Chem. Lett. 2015, 6, 1954−1960

electronic coherence exists, $\Delta A_{iso}(t)$ does not show any oscillations, while $r(t)$ shows obvious oscillation. In case (2), where only vibrational coherence exists, $\Delta A_{iso}(t)$ shows oscillations due to the underdamped vibrational motion, whereas $r(t)$ does not show any oscillations because there is no energy transfer between the two monomers. Results of case (3) are most interesting: Although the individual $\Delta A_{\parallel}(t)$ and $\Delta A_{\perp}(t)$ signals show complex oscillatory patterns due to the strong electronic coupling and the underdamped vibration, the isotropic pump−probe signal $\Delta A_{iso}(t)$ shows simple oscillation similar to the one in case (2), where only vibrational coherence exists. The anisotropy decay signal $r(t)$ shows more complicated oscillations, which implies it is affected by both the electronic coupling and the underdamped vibrational motion, that is, the vibronic coherence. It can be observed that the isotropic pump−probe signals in cases (2) and (3) are in phase, indicating that $\Delta A_{iso}(t)$ is more sensitive to the vibrational motion, while the anisotropy decay signals in cases (1) and (3) become out of phase at longer times, indicating that $r(t)$ in case (3) is also modulated by the vibrational motion. We note that the different characteristics in the pump−probe polarization anisotropy signals are due to whether the given spectral density describes overdamped or underdamped vibrational motion. Simulations with more complex spectral densities calculated from realistic systems[21,35,36] with a combination of overdamped and underdamped modes should lead to similar characteristic signals as in the above three cases.

The above analyses thus show that because the isotropic pump−probe signal $\Delta A_{iso}(t)$ and the anisotropy decay $r(t)$ are sensitive to different types of quantum coherence, the results of pump−probe polarization anisotropy experiments can be used to distinguish them. Namely, the isotropic pump−probe signal is sensitive to the vibrational and vibronic coherence, which needs an underdamped vibrational mode with a reasonable large electron−phonon coupling to show quantum beats. On the other hand, the anisotropy decay signal reflects the energy transfer between molecules with different dipole orientations, so oscillations in $r(t)$ should be caused by electronic or vibronic coherence. Thus, by observing the different oscillatory patterns in $\Delta A_{iso}(t)$ and $r(t)$, the specific type of quantum coherence behind the observed quantum beats can be determined.

Finally, we investigate whether an undamped harmonic oscillator with a small Huang−Rhys factor can lead to observable oscillations in the pump−probe polarization anisotropy signals. For this purpose, we take a dimer model consisting of pigments 3 and 4, the two monomers in the FMO complex with the lowest site energies, using the following parameters: ϵ = 175 cm^{-1}, J = −62 cm^{-1}. The electronic-vibrational coupling in the dimer is modeled with a combination of Debye spectral density with η = 70 cm^{-1} and ω_c^{-1} = 100 fs^{-1} and an additional undamped vibrational mode whose frequency and Huang−Rhys factor are to be specified later. The temperature is 19 K, and the fwhm of the laser pulses is 87 fs, which is the same as in the experiment.[24]

Frequencies and Huang−Rhys factors of the vibrational modes for the Q_y transition of the Bchla molecule are available from previous experiments,[20,41] where the largest Huang−Rhys factor is no more than 0.05. We perform simulations with two different vibrational frequencies ω_v = 700 cm^{-1} (several vibrational modes with frequency near 700 cm^{-1} are shown to have Huang−Rhys factors close to 0.05 in ref 41) and 400 cm^{-1}. The simulated isotropic pump−probe signal $\Delta A_{iso}(t)$ and anisotropy decay $r(t)$ with different Huang−Rhys factors are shown in Figures 5 and 6. The results for ω_v = 700 cm^{-1} in Figure 5 show that despite some small changes of the amplitude

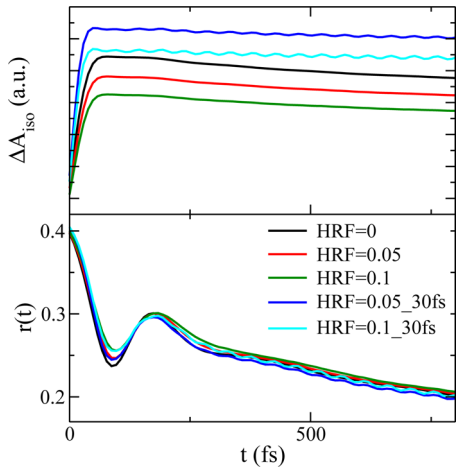

Figure 5. Isotropic pump−probe signal $\Delta A_{iso}(t)$ and anisotropy decay $r(t)$ for the model of the dimer consisting of pigment 3 and 4 of FMO complex. The frequency of the undamped vibrational mode is 700 cm^{-1}. Results with different values of the Huang−Rhys factors (HRFs) are shown, and the fwhm of the laser pulse is 87 fs, except for the last two curves with fwhm of 30 fs, which are labeled in the Figure.

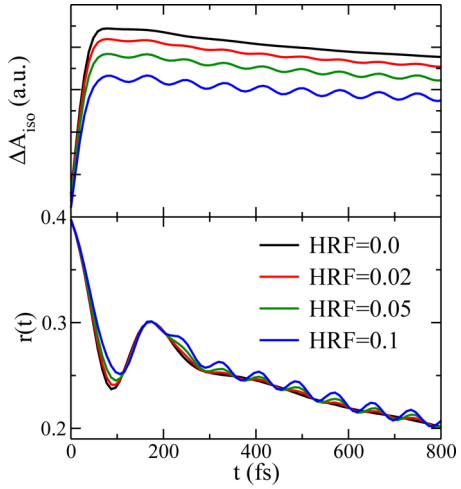

Figure 6. Same as 5, with the frequency of the undamped vibrational mode ω_v = 400 cm^{-1}.

of the curves the main shapes of $\Delta A_{iso}(t)$ and $r(t)$ stay the same with Huang−Rhys factor up to 0.1, and no new oscillatory features due to the vibrational mode can be observed. On the contrary, the results for ω_v = 400 cm^{-1} in Figure 6 show that an undamped vibrational mode with a Huang−Rhys factor of 0.05 can cause observable quantum beats within a much longer time. We can also see from Figure 6 that $\Delta A_{iso}(t)$ is dominated by vibrational coherence, while $r(t)$ shows electronic coherence at short time and is dominated by vibrational coherence at longer times.

The difference between the two cases with ω_v = 700 and 400 cm^{-1} should be due to the fact that the pump pulse is not short enough to excite simultaneously more than one vibrational level when ω_v = 700 cm^{-1}. To further confirm this point, we use shorter laser pulses with fwhm of 30 fs to simulate the dimer model with ω_v =700 cm^{-1} and the Huang−Rhys factors 0.05 and 0.1. The results are shown in Figure 5, where long time

DOI: 10.1021/acs.jpclett.5b00690
J. Phys. Chem. Lett. 2015, 6, 1954−1960

quantum beats can be observed in both the isotropic pump−probe signal $\Delta A_{iso}(t)$ and the anisotropy decay $r(t)$.

Although we have employed a simplified dimer model to investigate the effect of undamped vibrational modes, the above simulation can be used to explain the experimental result that no long time oscillations from vibrational coherence was observed in ref 24. Several vibrational modes above 700 cm^{-1} have Huang−Rhys factors close to 0.05,[20,41] but they are not effectively excited with the experimental setup. At the same time, the Huang−Rhys factors of vibrational modes with frequency smaller than 700 cm^{-1} in the FMO complex are significantly smaller than 0.05, which means they can not cause obvious oscillation in the experiment.

According to the findings above, if the laser pulses are short enough to effectively cover the vibrational modes of higher frequencies (>700 cm^{-1}) with larger Huang−Rhys factors, long time vibronic coherence should be observed in the pump−probe polarization anisotropy experiment of the FMO complex. This agrees with the conclusion in the recent work of Johnson et al. that the derivative of oscillatory signal to the pulse duration time in impulsive limit can be used as practical witness to discriminate the coherence.[42] The conclusion is also supported by recent work of Tempelaar et al., where they have found that quantum beating from electronic coherence in 2D spectra is limited to <500 fs, while the beating from vibrational coherence will last much longer.[18] It also means that even for the same system, the difference of laser pulses used in the pump−probe experiment may lead to observation of different types of coherences. The effect of laser pulse width should also be relevant to the observation of vibrational coherences in recent 2D spectroscopy studies of photosynthetic complexes.[4−9] In comparison with the pump−probe polarization decay study in ref 24, the much shorter laser pulses used in these works make it much easier to observe quantum beats caused by the vibronic coherence, which is also consistent with the conclusion in the recent work of Plenio et al. that contributions of electronic and vibronic coherence to the signals may be of the same order in realistic parameter regimes.[43]

To summarize, we have simulated the ultrafast pump−probe polarization anisotropy of the models from photosynthetic light-harvesting complexes with different types of quantum coherence. The coherence time from the FMO complex model with only electronic coherence at 19 K agrees well with the experiment and implies that the electronic coherence should be dominant in this experiment. Simulations of dimer models then show that three types of quantum coherence, including electronic, vibrational, and vibronic coherences, can be effectively differentiated from the results of pump−probe polarization anisotropy decay. More specifically, oscillations in the isotropic pump−probe signal $\Delta A_{iso}(t)$ are sensitive to the existence of vibrational or vibronic coherence, and oscillations in the anisotropy decay $r(t)$ are mainly due to the electronic or vibronic coherence. Finally, we simulate a dimer taken from FMO complex model with an undamped vibrational mode, and the results show that the oscillations from the vibronic coherence mode with a Huang−Rhys factor larger than 0.05 might be observable, provided that the detuning and width of the laser pulses allow simultaneous excitation of more than one vibrational state. This result also agrees with the recent works of Romero et al.[9] and Fujihashi et al.,[17] where they found that vibrational modes with small Huang−Rhys factors can contribute to the enhanced long-lived quantum beating in the 2D electronic spectra. The above findings thus offer a new explanation of the discrepant results in previous studies of FMO complex and may inspire the design of new experiments to analyze quantum coherence in photosynthetic light-harvesting complexes.

METHODS AND COMPUTATIONAL DETAILS

The Frenkel exciton model of coupled two-state chromophores is used to describe the aggregates of Bchla pigments in the photosynthetic light-harvesting complexes.[1,2] The molecular Hamiltonian H_{mol} is given by

$$H_{mol} = H_e + H_{ph} + H_{e-ph} \tag{1}$$

In the above equation, H_e describes the electronic degrees of freedom

$$H_e = \sum_{m=1}^{N} \epsilon_m a_m^+ a_m + \sum_{m=1}^{N} \sum_{n<m} J_{nm}(a_m^+ a_n + a_n^+ a_m) \tag{2}$$

where ϵ_m is the site energy of the mth molecule and a_m^+ and a_m are the creation and annihilation operators of the electronic transition on the mth molecule. Because of the energy mismatches, we ignore the effects from higher excited states on pump−probe signals, which should suffice in this work. H_{ph} describes the nuclear (phonon) degrees of freedom

$$H_{ph} = \sum_{m=1}^{N} \sum_{j=1}^{N_b^m} \left(\frac{p_{mj}^2}{2} + \frac{1}{2}\omega_{mj} x_{mj}^2 \right) \tag{3}$$

where N_b^m is the number of bath modes coupled to molecule m and x_{mj} and p_{mj} are the position and momentum of the jth harmonic oscillator bath mode with frequency ω_{mj}. The electron−phonon (or electronic−vibrational) coupling term H_{e-ph} causes site energy fluctuations that are independent for each molecule

$$H_{e-ph} = \sum_{m=1}^{N} \sum_{j=1}^{N_b^m} c_{mj} x_{mj} a_m^+ a_m = \sum_{m=1}^{N} F_m a_m^+ a_m \tag{4}$$

where the collective bath coordinate F_m is defined as $F_m = \sum_{j=1}^{N_b^m} c_{mj} x_{mj}$. The system−bath interaction is characterized by the spectral density $J(\omega)$ defined as

$$J(\omega) = \frac{\pi}{2} \sum_j \frac{c_j^2}{\omega_j} \delta(\omega - \omega_j) \tag{5}$$

In this study, $J(\omega)$ is assumed to be the same for all monomers, and two types of spectral densities are used to describe overdamped and underdamped vibrational motion, respectively. For the overdamped vibrational motion, the Debye type spectral density is used

$$J(\omega) = \frac{\eta \omega_c \omega}{\omega^2 + \omega_c^2} \tag{6}$$

which assumes exponential decay of the correlation function of the energy gap fluctuations in the high-temperature limit. In eq 6, η describes the electron−phonon coupling strength, with the reorganization energy $\lambda = \eta/2$, and ω_c^{-1} is the exponentially decaying time constant for the bath correlation function. For the underdamped vibrational motion, a Lorentzian type spectral density is used

DOI: 10.1021/acs.jpclett.5b00690
J. Phys. Chem. Lett. 2015, 6, 1954−1960

$$J(\omega) = \frac{2\eta\gamma(\omega_0^2 + \gamma^2)\omega}{[(\omega + \omega_0)^2 + \gamma^2][(\omega - \omega_0)^2 + \gamma^2]} \quad (7)$$

The Lorentzian spectral density describes an underdamped harmonic oscillator whose correlation function oscillates with frequency ω_0 and a decaying constant γ. We also have $\lambda = \eta/2$ for eq 7. The undamped vibrational mode is considered by using a single vibrational mode in eq 5: $J(\omega) = \pi\lambda\omega_0\delta(\omega - \omega_0)$, where ω_0 is the vibrational frequency, and the reorganization energy $\lambda = S\hbar\omega_0$, where the Huang–Rhys factor $S = c^2/2\hbar\omega_0^3$.

We simulate the pump–probe polarization anisotropy signals using the nonperturbative scheme developed by Seidner et al.,[44] which calculates the molecular response directly in the presence of the electromagnetic field, and extract the desired pump–probe signal by combining results of pump–probe pulse pairs with different phase differences. The overall molecular polarization under the influence of the pump and probe pulses is first calculated, and molecular polarizability $\boldsymbol{P}_{pp}$ responsible for the pump–probe signal is obtained from four overall polarization $\boldsymbol{P}(\phi)s$ with different phase difference ϕ between the pump and probe pulses[44]

$$\boldsymbol{P}_{pp} = \frac{1}{2}Re\{\boldsymbol{P}(0) + \boldsymbol{P}(\pi/2) + \boldsymbol{P}(\pi) + \boldsymbol{P}(3\pi/2)\} \quad (8)$$

The pump–probe signal is then given by

$$\Delta A_{pp}(\tau) = \int_{-\infty}^{+\infty} dt\ \dot{\boldsymbol{E}}_2(t)\cdot(\boldsymbol{P}_{\text{pump on}}(t) - \boldsymbol{P}_{\text{pump off}}(t)) \quad (9)$$

where $\boldsymbol{E}_2$ is the electric field of the probe pulse, $\boldsymbol{P}$ is the molecular polarizability defined in eq 8, and τ is the time delay between the pump and probe pulses.

The parallel and perpendicular pump–probe signals $\Delta A_{\parallel}(t)$ and $\Delta A_{\perp}(t)$ are calculated with the pump and probe electric filed parallel and perpendicular to each other, respectively. The following isotropic pump–probe and anisotropy decay signals are defined using $\Delta A_{\parallel}(t)$ and $\Delta A_{\perp}(t)$

$$\Delta A_{\text{iso}}(t) = \Delta A_{\parallel}(t) + 2\Delta A_{\perp}(t) \quad (10)$$

$$r(t) = \frac{\Delta A_{\parallel}(t) - \Delta A_{\perp}}{\Delta A_{\parallel}(t) + 2\Delta A_{\perp}(t)} \quad (11)$$

In the simulations, a total number of 1000 averages were used in each calculation to model the static and orientational disorders. The static energetic disorders are found to be important in determining the absorption line shape and the amplitude of quantum beats from the electronic coherence, but have rather indirect effects on the beating signals from the vibrational coherence. As in typical experiments of the photosynthetic complexes, we assume that orientations of the monomers do not change during the observation time.

We apply the HEOM method[45−50] to simulate the dissipative quantum dynamics under the ultrafast electromagnetic field. Details of the HEOM calculations can be referred to our previous work.[23] The protocol to treat the various spectral densities within the HEOM framework can be found in ref 51. To facilitate the HEOM simulation of the FMO complex at the experimental temperature at 19 K, we use the dynamic filtering method in ref 50 and the Padé approximation to decompose the bath correlation functions at low temperatures.[52] In comparison with previous studies by Zhu et al. also using the HEOM method,[53] our method here is nonperturbative to the treatment of light–molecule interactions as well as the dissipative baths. So the accuracy of the simulation is only limited by the validity of the model Hamiltonian without further approximations.

AUTHOR INFORMATION

Corresponding Author

*E-mail: qshi@iccas.ac.cn.

Notes

The authors declare no competing financial interest.

ACKNOWLEDGMENTS

This work is supported by NSFC (grant no. 21290194), the 973 program (grant nos. 2011CB808502 and 2013CB933501), and the Strategic Priority Research Program of the Chinese Academy of Sciences (grant no. XDB12020300).

REFERENCES

(1) *Photosythetic Exictons*; van Amerongen, H., Valkunas, L., van Grondelle, R., Eds.; World Scientific: Singapore, 2000.

(2) Cheng, Y.-C.; Fleming, G. R. Dynamics of Light Harvesting in Photosynthesis. *Annu. Rev. Phys. Chem.* **2009**, *60*, 241–262.

(3) Kim, H. W.; Kelly, A.; Park, J. W.; Rhee, Y. M. All-Atom Semiclassical Dynamics Study of Quantum Coherence in Photosynthetic Fenna-Matthews-Olson Complex. *J. Am. Chem. Soc.* **2012**, *134*, 11640–51.

(4) Engel, G. S.; Calhoun, T. R.; Read, E. L.; Ahn, T.-K.; Mancal, T.; Cheng, Y.-C.; Blankenship, R. E.; Fleming, G. R. Two-Dimensional Spectroscopy of Electronic Couplings in Photosynthesis. *Nature* **2007**, *446*, 782.

(5) Collini, E.; Wong, C. Y.; Wilk, K. E.; Curmi, P. M. G.; Brumer, P.; Scholes, G. D. Coherently Wired Light-Harvesting in Photosynthetic Marine Algae at Ambient Temperature. *Nature* **2010**, *463*, 644–647.

(6) Panitchayangkoon, G.; Hayes, D.; Fransted, K. A.; Caram, J. R.; Harel, E.; Wen, J.; Blankenship, R. E.; Engel, G. S. Long-Lived Quantum Coherence in Photosynthetic Complexes at Physiological Temperature. *Proc. Natl. Acad. Sci. U.S.A.* **2010**, *107*, 12766.

(7) Westenhoff, S.; Palecek, D.; Edlund, P.; Smith, P.; Zigmantas, D. Coherent Picosecond Exciton Dynamics in a Photosynthetic Reaction Center. *J. Am. Chem. Soc.* **2012**, *134*, 16484–7.

(8) Fuller, F. D.; Pan, J.; Gelzinis, A.; Butkus, V.; Senlik, S. S.; Wilcox, D. E.; Yocum, C. F.; Valkunas, L.; Abramavicius, D.; Ogilvie, J. P. Vibronic Coherence in Oxygenic Photosynthesis. *Nat. Chem.* **2014**, *6*, 706–711.

(9) Romero, E.; Augulis, R.; Novoderezhkin, V. I.; Ferretti, M.; Thieme, J.; Zigmantas, D.; van Grondelle, R. Quantum Coherence in Photosynthesis for Efficient Solar-Energy Conversion. *Nat. Phys.* **2014**, *10*, 676–682.

(10) Hildner, R.; Brinks, D.; Nieder, J. B.; Cogdell, R. J.; van Hulst, N. F. Quantum Coherent Energy Transfer over Varying Pathways in Single Light-Harvesting Complexes. *Science* **2013**, *340*, 1448–1451.

(11) Ishizaki, A.; Fleming, G. R. Theoretical Examination of Quantum Coherence in a Photosynthetic System at Physiological Temperature. *Proc. Natl. Acad. Sci. U.S.A.* **2009**, *106*, 17255.

(12) Tiwari, V.; Peters, W. K.; Jonas, D. M. Electronic Resonance with Anticorrelated Pigment Vibrations Drives Photosynthetic Energy Transfer Outside the Adiabatic Framework. *Proc. Natl. Acad. Sci. U.S.A.* **2013**, *110*, 1203–1208.

(13) Chin, A. W.; Prior, J.; Rosenbach, R.; Caycedo-Soler, F.; Huelga, S. F.; Plenio, M. B. The Role of Non-Equilibrium Vibrational Structures in Electronic Coherence and Recoherence in Pigment-Protein Complexes. *Nat. Phys.* **2013**, *9*, 113–118.

(14) Christensson, N.; Kauffmann, H. F.; Pullerits, T.; Mancal, T. Origin of Long-Lived Coherences in Light-Harvesting Complexes. *J. Phys. Chem. B* **2012**, *116*, 7449–7454.

DOI: 10.1021/acs.jpclett.5b00690
J. Phys. Chem. Lett. 2015, 6, 1954–1960

(15) Womick, J. M.; Moran, A. M. Vibronic Enhancement of Exciton Sizes and Energy Transport in Photosynthetic Complexes. *J. Phys. Chem. B* **2011**, *115*, 1347−1356.
(16) Dijkstra, A. G.; Wang, C.; Cao, J. S.; Fleming, G. R. Coherent Exciton Dynamics in the Presence of Underdamped Vibrations. *J. Phys. Chem. Lett.* **2015**, *6*, 627−632.
(17) Fujihashi, Y.; Fleming, R.; A, I. Impact of Environmentally Induced Fluctuations on Quantum Mechanically Mixed Electronic and Vibrational Pigment States in Photosynthetic Energy Transfer and 2D Electronic Spectra. *J. Chem. Phys.* **2015**, *142*, 212403.
(18) Tempelaar, R.; Jansen, T. L. C.; Knoester, J. Vibrational Beatings Conceal Evidence of Electronic Coherence in the FMO Light-Harvesting Complex. *J. Phys. Chem. B* **2014**, *118*, 12865−12872.
(19) Halpin, A.; Johnson, P. J. M.; Tempelaar, R.; Murphy, R. S.; Knoester, J.; Jansen, T. L. C.; Miller, R. J. D. Two-Dimensional Spectroscopy of a Molecular Dimer Unveils the Effects of Vibronic Coupling on Exciton Coherences. *Nat. Chem.* **2014**, *6*, 196−201.
(20) Cherepy, N.; Shreve, A.; Moore, L.; Boxer, S.; Mathies, R. Electronic and Nuclear Dynamics of the Accessory Bacteriochlorophylls in Bacterial Photosynthetic Reaction Centers from Resonance Raman Intensities. *J. Phys. Chem. B* **1997**, *101*, 3250−3260.
(21) Jing, Y.-Y.; Zheng, R.-H.; Li, H.-X.; Shi, Q. Theoretical Study of the Electronic-Vibrational Coupling in the Q_y States of the Photosynthetic Reaction Center in Purple Bacteria. *J. Phys. Chem. B* **2012**, *116*, 1164.
(22) Fransted, K. A.; Caram, J. R.; Hayes, D.; Engel, G. S. Two-Dimensional Electronic Spectroscopy of Bacteriochlorophyll A in Solution: Elucidating the Coherence Dynamics of the Fenna-Matthews-Olson Complex Using Its Chromophore as a Control. *J. Chem. Phys.* **2012**, *137*.
(23) Chen, L.-P.; Zheng, R.-H.; Jing, Y.-Y.; Shi, Q. Simulation of the Two-Dimensional Electronic Spectra of the Fenna-Matthews-Olson Complex Using the Hierarchical Equations of Motion Method. *J. Chem. Phys.* **2011**, *134*, 194508.
(24) Savikhin, S.; Buck, D. R.; Struve, W. S. Oscillating Anisotropies in a Bacteriochlorophyll Protein: Evidence for Quantum Beating Between Exciton Levels. *Chem. Phys.* **1997**, *223*, 303−312.
(25) Smith, E. R.; Farrow, D. A.; Jonas, D. M. Response Functions for Dimers and Square-Symmetric Molecules in Four-Wave-Mixing Experiments with Polarized Light. *J. Chem. Phys.* **2005**, *123*, 044102.
(26) Farrow, D. A.; Qian, W.; Smith, E. R.; Ferro, A. A.; Jonas, D. M. Polarized Pump-Probe Measurements of Electronic Motion via a Conical Intersection. *J. Chem. Phys.* **2008**, *128*, 144510.
(27) Yuen-Zhou, J.; Krich, J. J.; Aspuru-Guzik, A. A Witness for Coherent Electronic vs Vibronic-only Oscillations in Ultrafast Spectroscopy. *J. Chem. Phys.* **2012**, *136*, 234501.
(28) Renger, T.; May, V. Ultrafast Exciton Motion in Photosynthetic Antenna Systems: The FMO-Complex. *J. Phys. Chem. A* **1998**, *102*, 4381−4391.
(29) Vulto, I. E.; de Baat, M. A.; Louwe, R. J. W.; Permentier, H. P.; Neef, T.; Miller, M.; van Amerongen, H.; Aartsma, T. J. Exciton Simulations of Optical Spectra of the FMO Complex from the Green Sulfur Bacterium Chlorobium tepidum at 6 K. *J. Phys. Chem. B* **1998**, *102*, 9577−9582.
(30) Cho, M.; Vaswani, H. M.; Brixner, T.; Stenger, J.; Fleming, G. R. Exciton Analysis in 2D Electronic Spectroscopy. *J. Phys. Chem. B* **2005**, *109*, 10542−10556.
(31) Lee, H.; Cheng, Y.-C.; Fleming, G. R. Coherence Dynamics in Photosynthesis: Protein Protection of Excitonic Coherence. *Science* **2007**, *316*, 1462.
(32) Sarovar, M.; Cheng, Y. C.; Whaley, K. B. Environmental Correlation Effects on Excitation Energy Transfer in Photosynthetic Light Harvesting. *Phys. Rev. E* **2011**, *83*, 011906.
(33) Huo, P.; Coker, D. F. Influence of Environment Induced Correlated Fluctuations in Electronic Coupling on Coherent Excitation Energy Transfer Dynamics in Model Photosynthetic Systems. *J. Chem. Phys.* **2012**, *136*.
(34) Curutchet, C.; Kongsted, J.; Munoz-Losa, A.; Hossein-Nejad, H.; Scholes, G. D.; Mennucci, B. Photosynthetic Light-Harvesting is Tuned by the Heterogeneous Polarizable Environment of the Protein. *J. Am. Chem. Soc.* **2011**, *133*, 3078−3084.
(35) Olbrich, C.; Struempfer, J.; Schulten, K.; Kleinekathoefer, U. Quest for Spatially Correlated Fluctuations in the FMO Light-Harvesting Complex. *J. Phys. Chem. B* **2011**, *115*, 758−764.
(36) Rivera, E.; Montemayor, D.; Masia, M.; Coker, D. F. Influence of Site-Dependent Pigment-Protein Interactions on Excitation Energy Transfer in Photosynthetic Light Harvesting. *J. Phys. Chem. B* **2013**, *117*, 5510−5521.
(37) Savikhin, S.; Buck, D. R.; Struve, W. S. Pump-probe Anisotropies of Fenna-Matthews-Olson Protein Trimers From Chlorobium Tepidum: A Diagnostic for Exciton Localization? *Biophys. J.* **1997**, *73*, 2090−2096.
(38) Lebedev, M. V.; Misochko, O. V.; Dekorsy, T.; Georgiev, N. On the Nature of "Coherent Artifact. *J. Exp. Theor. Phys.* **2005**, *100*, 272−282.
(39) Dietzek, B.; Pascher, T.; Sundstrom, V.; Yartsev, A. Appearance of Coherent Artifact Signals in Femtosecond Transient Absorption Spectroscopy in Dependence on Detector Design. *Laser Phys. Lett.* **2007**, *4*, 38−43.
(40) Devos, O.; Mouton, N.; Sliwa, M.; Ruckebusch, C. Baseline Correction Methods to Deal with Artifacts in Femtosecond Transient Absorption Spectroscopy. *Anal. Chim. Acta* **2011**, *705*, 64−71.
(41) Pullerits, T.; Hess, S.; Herek, J. L.; Sundstrom, V. Temperature Dependence of Excitation Transfer in LH2 of Rhodobacter Sphaeroides. *J. Phys. Chem. B* **1997**, *101*, 10560−10567.
(42) Johnson, A. S.; Yuen-Zhou, J.; Aspuru-Guzik, A.; Krich, J. J. Practical Witness for Electronic Coherences. *J. Chem. Phys.* **2014**, *141*, 244109.
(43) Plenio, M. B.; Almeida, J.; Huelga, S. F. Origin of Long-Lived Oscillations in 2D-spectra of a Quantum Vibronic Model: Electronic versus Vibrational Coherence. *J. Chem. Phys.* **2013**, *139*, 235102.
(44) Seidner, L.; Stock, G.; Domcke, W. Nonperturbative Approach to Femtosecond Spectroscopy: General Theory and Application to Multidimensional Nonadiabatic Photoisomerization Processes. *J. Chem. Phys.* **1995**, *103*, 3998−4011.
(45) Tanimura, Y.; Kubo, R. K. Time Evolution of a Quantum System in Contact with a Nearly Gaussian-Markoffian Noise Bath. *J. Phys. Soc. Jpn.* **1989**, *58*, 101.
(46) Tanimura, Y. Stochastic Liouville, Langevin, Fokker-Planck, and Master Equation Approaches to Quantum Dissipative Systems. *J. Phys. Soc. Jpn.* **2006**, *75*, 082001−082039.
(47) Yan, Y.; Yang, F.; Liu, Y.; Shao, J. Hierarchical Approach Based on Stochastic Decoupling to Dissipative Systems. *Chem. Phys. Lett.* **2004**, *395*, 216.
(48) Xu, R.-X.; Cui, P.; Li, X.-Q.; Mo, Y.; Yan, Y.-J. Exact Quantum Master Equation via the Calculus on Path Integrals. *J. Chem. Phys.* **2005**, *122*, 041103.
(49) Ishizaki, A.; Tanimura, Y. Quantum Dynamics of System Strongly Coupled to Low-Temperature Colored Noise Bath: Reduced Hierarchy Equations Approach. *J. Phys. Soc. Jpn.* **2005**, *74*, 3131−3134.
(50) Shi, Q.; Chen, L. P.; Nan, G. J.; Xu, R. X.; Yan, Y. J. Efficient Hierarchical Liouville-Space Propagator to Quantum Dissipative Dynamics. *J. Chem. Phys.* **2009**, *130*, 084105−084108.
(51) Liu, H.; Zhu, L.; Bai, S.; Shi, Q. Reduced Quantum Dynamics with Arbitrary Bath Spectral Densities: Hierarchical Equations of Motion Based on Several Different Bath Decomposition Schemes. *J. Chem. Phys.* **2014**, *140*, 134106.
(52) Hu, J.; Xu, R. X.; Yan, Y. J. Padé Spectrum Decomposition of Fermi Function and Bose Function. *J. Chem. Phys.* **2010**, *133*, 101106.
(53) Zhu, K.-B.; Xu, R.-X.; Zhang, H. Y.; Hu, J.; Yan, Y. J. Hierarchical Dynamics of Correlated System-Environment Coherence and Optical Spectroscopy. *J. Phys. Chem. B* **2011**, *115*, 5678−5684.

DOI: 10.1021/acs.jpclett.5b00690
J. Phys. Chem. Lett. 2015, 6, 1954−1960